# Discovery of kHz QPOs and shifted frequency correlations in the accreting millisecond pulsar XTE J1807–294

Manuel Linares<sup>1</sup>, Michiel van der Klis<sup>1</sup>, Diego Altamirano<sup>1</sup>, Craig B. Markwardt<sup>2,3</sup>

## **ABSTRACT**

We report the discovery of twin kHz QPOs in the X ray flux of XTE J1807–294, the fourth accreting millisecond pulsar (AMP). This is the second AMP exhibiting twin kHz QPOs. In contrast to the first case, SAX J1808.4–3658, the frequency separation  $\Delta\nu$  between the kHz QPOs is consistent with the pulse frequency (190.6 Hz), not with half that value, confirming for the first time from pulsation measurements the inference, based on burst oscillations, that 'slow rotators' (spin frequency less than 400 Hz) have  $\Delta\nu$  approximately equal to the spin frequency. While the QPOs move in frequency together over a range of more than 200 Hz,  $\Delta\nu$  remains constant with an average value of 205±6 Hz. Variability components were found in the 5–130 Hz range similar to those seen in other LMXBs. The correlations between the QPO and noise frequencies are also similar to those in other sources, but shifted by a factor of 1.59 in kHz QPO frequencies, similar to the factor 1.45 shift found for SAX J1808.4–3658. Our results argue in favour of a spin-related formation mechanism for twin kHz QPOs and against a spin-related cause of the shift in the frequency correlations.

Subject headings: binaries: close — pulsars: individual (XTE J1807–294) — stars: neutron — X-rays: binaries

## 1. Introduction

The accretion-driven millisecond X-ray pulsar (AMP) family is gradually growing. Since the discovery of its first member (SAX J1808.4–3658, Wijnands & van der Klis 1998) six more have been added: XTE J1751–305, XTE J0929–314, XTE J1807–294, XTE J1814–338 and

<sup>&</sup>lt;sup>1</sup>Astronomical Institute "Anton Pannekoek," University of Amsterdam and Center for High-Energy Astrophysics, Kruislaan 403, NL-1098 SJ Amsterdam, Netherlands.

<sup>&</sup>lt;sup>2</sup>Laboratory for High Energy Astrophysics, NASA Goddard Space Flight Center, Greenbelt, MD 20771.

<sup>&</sup>lt;sup>3</sup>Department of Astronomy, University of Maryland, College Park, MD 20742.

recently IGR J00291+5934 and HETE J1900.1–2455 (respectively: Markwardt et al. 2002; Remillard 2002; Markwardt et al. 2003a; Markwardt & Swank 2003; Galloway et al. 2005; Vanderspek et al. 2005). All of these are in transient low-mass X-ray binaries (LMXBs) showing faint outbursts (peak count rate 10–100 mCrab) every few years that last a few weeks. Their pulse frequency (i.e., the neutron-star spin frequency) lies in the range 185–599 Hz and the orbital period is between 40 minutes and 2.5 hours. See Wijnands (2005) for an updated observational review.

XTE J1807–294 is the fourth-discovered accreting millisecond pulsar. The source was detected first on February  $13^{th}$ , 2003, in periodic scans of the Galactic bulge region using the Proportional Counter Array (PCA) instrument on board the Rossi X-ray Timing Explorer (RXTE). These scanning observations show a rising flux, with the epoch of maximum X-ray flux (count rate of  $\sim 58$  mCrab) occurring between February  $19^{th}$  and  $22^{nd}$  (Markwardt et al. 2003b). On February  $21^{st}$ , 2003, in the first pointed observation of the source by the PCA, 190.6 Hz pulsations were detected, confirming this source as an accreting millisecond pulsar (Markwardt et al. 2003b). An orbital period of  $\sim 40$  minutes was determined by Markwardt et al. (2003a), still the shortest among AMPs. A pulse analysis of the outburst was performed by Markwardt (2004).

XTE J1807–294 had the longest outburst among the AMPs observed up to now. It was followed with the PCA for five months, although after a few weeks the source became too weak to measure its aperiodic variability. As noted in Falanga et al. (2005), the X-ray flux decay did not show a break to a faster decline, such as in the other AMPs (Wijnands 2005) and attributed in those objects to the propeller effect (e.g., Gilfanov et al. 1998). Falanga et al. (2005) described the energy spectrum as a sum of a disk blackbody and a thermal Comptonization component, without evidence of spectral lines or reflection. No optical or infrared counterpart has been reported to date. Assuming a distance of 8kpc, Campana et al. (2005) placed an upper limit of  $4\times10^{31}$  erg  $s^{-1}$  on the unabsorbed 0.5–10 keV quiescent luminosity.

Studying the power spectra of LMXBs is one of the most direct ways of analyzing the accretion flow in these systems. In particular the high-frequency power-spectral features constitute a probe of the innermost regions of the accretion disk, where gravitational fields are extreme (see van der Klis 2000, 2004, for reviews). The first discovered AMP, SAX J1808.4–3658 (Wijnands & van der Klis 1998), in its 2002 outburst provided surprising information on the relation between the neutron-star spin and the kHz QPOs and confirmed expectations concerning the burst oscillations. While the burst oscillations (cf. Strohmayer et al. 1996) occurred at the pulse, and inferred spin, frequency (Chakrabarty et al. 2003), the separation  $\Delta\nu$  between the kHz QPO frequencies was consistent with half the pulse frequency (Wijnands

et al. 2003). Although based on only a single simultaneous detection of twin kHz QPOs, this result carried important consequences for our understanding of LMXBs, as it falsifies simple spin-orbit beat-frequency models, yet requires an intimate link between spin and kHz QPOs. This led to several new proposed models for the nature of the interaction between disk flow and neutron-star spin (Wijnands et al. 2003; Lamb & Miller 2003; Kluźniak et al. 2004; Lee et al. 2004) replacing, modifying or adding to earlier proposed models (e.g., Miller et al. 1998; Stella & Vietri 1998; Abramowicz et al. 2003). So far, all sources with inferred spin frequencies  $\nu_{spin} > 400$  Hz ('fast rotators') have  $\Delta \nu \approx \nu_{spin}/2$  and the ones with  $\nu_{spin} < 400$  Hz ('slow rotators') have  $\Delta \nu \approx \nu_{spin}$ .

Several correlations have been found between the frequencies of power-spectral components in Z and atoll sources (the two main types of neutron-star LMXBs; Hasinger & van der Klis 1989), as well as among black hole candidate systems. Initially, the WK relation (Wijnands & van der Klis 1999) and the PBK relation (Psaltis et al. 1999) were identified. Including several more correlated components, this set of correlations was synthesized into a 'universal scheme of correlations' among atoll sources by van Straaten et al. (2003). Comparing AMPs to other atoll sources, van Straaten et al. (2005) found that the correlations in two of the AMPs are shifted relative to those of the other atoll sources. The simplest description of the shifts was that the two kHz QPOs had frequencies a factor  $\sim 1.5$  lower than in the other sources.

In this paper we analyze all the RXTE PCA data on XTE J1807–294, and report the discovery of pairs of simultaneous kHz QPOs. The separation  $\Delta\nu$  between the seven pairs of kHz QPOs we detect is consistent with the pulse frequency, and confirms for the first time from pulsations that the slow rotators have a kHz QPO frequency separation that is approximately equal to the neutron star spin frequency. Finally, including also the low-frequency variability components in our study, we find a shift in the frequency correlations by a factor  $\sim 1.5$ , similar to that seen in SAX J1808.4–3658.

## 2. Observations and Data Analysis

We used all the RXTE PCA data from XTE J1807–294 available in NASA's High Energy Astrophysics Science Archive Research Center taken between February 27<sup>th</sup> and July 29<sup>th</sup>, 2003.

For the color analysis we used the Standard 2 data, which have a 16-s time resolution and 129 energy channels. We divided the channels into four bands in a way that is often used for neutron-star sources: band A: 2.0–3.5 keV, band B: 3.5–6.0 keV, band C: 6.0–9.7 keV,

band D: 9.7–16.0 keV. The count rates in these precise bands were estimated by interpolating linearly between the corresponding energy channels. The background was estimated using the standard bright source background models. From the counts in each band, we computed the colors and intensity as: hard color=D/C, soft color=B/A, intensity=A+B+C+D. We then normalized colors and intensity to the Crab values nearest in time (Kuulkers et al. 1994) and in the same PCA gain epoch (e.g., van Straaten et al. 2003).

The timing analysis was done using the GoodXenon data, with the original  $1\mu s$  time resolution data rebinned into 1/8192-s bins, and including all 256 energy channels. We performed fast Fourier transforms (FFTs) of 128-s data segments, fixing the frequency resolution and the lowest available frequency to  $\sim 0.008$  Hz; the highest available Fourier frequency (Nyquist frequency) was 4096 Hz. No background subtraction or dead-time correction was made prior to the FFTs. The resulting power spectra were "weeded" (the pulsar spike at  $\sim$  190 Hz was removed at full frequency resolution) and a Poisson level was subtracted. Following Klein-Wolt (2004) we first estimated the Poisson noise using the Zhang et al. (1995) formula and then (after inspecting the  $\sim 3000-4000$  Hz range and finding no unexpected features) shifted it to match the level between 3072–4096 Hz, where no intrinsic power should be present, but only counting statistics noise (this shift was in all cases smaller than 0.15% of the previously estimated Poisson level). Then we normalized the power spectra using the rms normalization (van der Klis 1995). Several observations with similar power spectra and colors were averaged into sets labeled A–H in order to improve the statistics (see Table 1). The sets were ordered by increasing kHz QPO frequencies.

To fit the overall broad-band power spectra we use a fit function consisting of the sum of several Lorentzians in the so-called " $\nu_{max}$  representation", described in Belloni et al. (2002). In this representation, if  $\nu_0$  is the Lorentzian's centroid frequency and  $\Delta$  its HWHM (half width at half maximum),  $\nu_{max} = \sqrt{\nu_0^2 + \Delta^2}$  gives the characteristic frequency of the feature (near the centroid if it is narrow and near the half-width if it is wide). The quality factor  $Q = \nu_0/2\Delta$  is a measure for the coherence of the variability feature. Its strength is given by the integral power whose square root, in the normalization we use, is the fractional rms amplitude of the variability. Four to five Lorentzian components were needed, all of them significant to more than  $3\sigma$ , with one exception noted in Table 3. In some cases in order to avoid a meaningless negative coherence, Q was fixed to zero, which is equivalent to fitting a zero-centered ( $\nu_0 = 0$ ) Lorentzian. From now on, consistent with previous work (e.g., Belloni et al. 2002; van Straaten et al. 2003; van der Klis 2004) we refer to these components as  $L_i$ , where the L stands for Lorentzian and 'i' is the label identifying the component ('b' for break, 'u' for upper kHz, 'l' for lower kHz, 'h' for hump, 'LF' for low frequency QPO). Following this notation we call  $L_i$ 's characteristic frequency  $\nu_i$  and its coherence  $Q_i$ . In order to measure the kHz QPO centroid frequencies and their frequency difference  $\Delta\nu$ , we performed exactly the same fits to the same data sets, now representing the Lorentzians' frequency by their centroid frequency  $\nu_{i,0}$ . While of course the two representations are mathematically equivalent, refitting was necessary to calculate the correct error bars for the frequencies. We split the sets in the original observations (see Table 1) and checked wether this led to a better measurement of  $\Delta\nu$ . Only in one case the statistical significance of the kHz QPOs increased (obs. 80145-01-03-00 in set H;  $\Delta\nu=197.8\pm7.6$  was closer to  $\nu_{spin}$ ) but in the final analysis we conservatively used the original datasets. Hereafter, when we talk about frequencies this refers always to characteristic frequencies ( $\nu_{max}$ ) as given above; whenever centroid frequencies ( $\nu_0$ ) are intended this is explicitly stated.

Power law functions were fitted to the  $\nu_i$  vs.  $\nu_u$  relations (where 'i' is one of the labels mentioned above) in order to quantify the correlations between these frequencies. For this, we used the FITEXY routine of Press et al. (1992) that takes into account errors in both coordinates and fitted straight lines to the  $\log \nu_i$  vs.  $\log \nu_u$  relations.

To quantify the shifts in the XTE J1807–294 correlations and compare them with the shifts in the other AMPs we used the same method as van Straaten et al. (2005): we took as a reference the atoll sources 4U 0614+09, 4U 1608–52, 4U 1728–34 and Aql X-1, and included only the frequency sets with  $\nu_u < 600$  Hz (as noted in van Straaten et al. (2005), the behavior of the power spectral components above that value becomes more complex; see also Section 4). We multiplied the upper kHz QPO frequencies of XTE J1807–294 by a factor f, which we varied between 0.01 and 5 with steps of 0.001. In each step we fitted a power law to the XTE J1807–294 and atoll source points together. The step with the best  $\chi^2$  gives us the optimal shift factor. We also calculated the shift factors in  $\nu_i$ , following exactly the same procedure, but multiplying the  $\nu_i$  instead of  $\nu_u$  by a factor f. In the above mentioned atoll sources there were only very few detections of  $L_{LF}$ . Therefore, to obtain some information about the shift in this component, we took as a reference the  $L_{LF1}$  component of the low luminosity bursters 1E 1724–3045 and GS 1826–24 (van Straaten et al. 2005), and again applied the same procedure.

#### 3. Results

Fig. 1 shows the light curve for all the observations, as well as the evolution in time of the soft and hard colors (for definitions see Section 2). As noted in Falanga et al. (2005) three peaks in the intensity occurred on March the  $9^{th}$ ,  $14^{th}$  and  $25^{th}$ ; a peak on March the  $30^{th}$  was instrumental (caused by a flare in PCU4) and removed in the current analysis. The overall trend in the colors is a gradual decline following a slight increase during the first two days of observations. The color-color and color-intensity diagrams are shown in Figs. 2

and 3, respectively. The region of the color diagrams spanned by the observations, as well as the overall shape of the power spectra (see below), is reminiscent of the island state in atoll sources (see van der Klis 2004). As can be seen from Figs. 1-3, there is a tendency for the colors to decrease with increasing QPO frequencies (from set A to set H), but the correspondence is not monotonic.

Two simultaneous kHz QPOs (see Fig. 4) were detected in seven of the eight datasets used in this paper; the best-fit centroid frequencies of these QPOs are listed in Table 2 together with centroid frequency differences and ratios. As discussed below, the identity of the Lorentzian below  $L_u$  is not clear in set A as it could be fitting either  $L_\ell$  or  $L_{hHz}$ , or both, so we did not include this value in the analysis of the kHz QPO centroid frequencies. The measured differences  $\Delta\nu$  between the kHz QPO centroid frequencies are consistent with being equal to the pulse, and inferred spin, frequency of 190.6 Hz (see Fig. 5), with no evidence for variations over the range the QPOs were detected. The weighted average of the seven values for  $\Delta\nu$  was 205.1±6.4 Hz, slightly (2.3 $\sigma$ ) higher than the pulse frequency.

The broad-band power spectra of the eight sets of observations can be seen in Fig. 6, with their multilorentzian fits. The  $\chi^2/\text{d.o.f.}$  of the fits were between 155/168 and 192/143. The best-fit parameters of the power spectral components are presented in Table 3.

The multilorentzian fits to the power spectra comprise a broad component at low frequencies (5–10 Hz),  $L_b$  (see Section 2 for nomenclature); two components at intermediate frequencies, one of them narrow at somewhat lower frequency and the other one wider and at higher frequency, respectively:  $L_{LF}$  (15–40 Hz) and  $L_h$  (25–130 Hz); and two narrow components at high frequencies (the kHz QPOs),  $L_{\ell}$  and  $L_{u}$  with characteristic frequencies 100–370 Hz and 340–570 Hz, respectively. In two of the sets (E and G)  $L_h$  was not detected, while in set H it has a frequency of  $\sim 130$  Hz and could also be identified as  $L_{hHz}$  (see van Straaten et al. 2002, 2003, 2005, for a description of this component in atoll sources and AMPs — the values of the correlation parameters given below do not change significantly when calculated excluding  $\nu_h$  in set H). The  $L_\ell$  of the two lowest frequency sets (A and B) are wider than the rest (Q $\sim$ 0.5 compared with Q $\sim$ 1.5) and in set A  $L_{\ell}$  lies slightly below the  $\nu_{\ell}$  vs.  $\nu_{u}$  correlation (see Fig. 7), suggesting that we may be looking at a blend between  $L_{\ell}$  and  $L_{hHz}$ . In set A we find a narrow Lorentzian (Q=8) at higher frequency (27 Hz) and a wider one (Q=1.4) at lower frequency (16 Hz). We call the higher-frequency one  $L_h$  and the lower-frequency one  $L_{LF}$ ; note that this implies  $Q_{LF} < Q_h$  for this data set. This choice has only a small effect on the numbers reported below and does not affect our conclusions. In the sets where  $L_h$  was not detected (E and G),  $Q_{LF}$  is also low, which might indicate that  $L_h$  and  $L_{LF}$  are blended.

The correlations between our measured characteristic frequencies are compared to those

in other sources in Fig. 7a. As in SAX J1808.4–3658, our source shows correlations that are shifted with respect to those of the atoll sources. Our results are closer to those of SAX J1808.4–3658 than to those of the other sources, but are somewhat different also from that source. The shift factors between the correlations in XTE J1807–294 and those in the atoll sources, calculated as explained in Section 2, are presented in Table 4. Note that due to the intrindic dispersion present in the frequency-frequency relations the reduced  $\chi^2$  $(\chi_r^2 = \chi^2/d.o.f.)$  is larger than 2 in three of the four shifts presented. We take this into account when deriving the errors by using  $\Delta \chi^2 = \chi_r^2$ . The  $L_b$  and  $L_h$  correlations show shifts in  $\nu_u$  by factors of 1.46±0.05 and 1.72±0.05, respectively. The lower kHz QPO can be made to match the atoll sources by shifting it by another factor ( $\sim 1.08$ ) in  $\nu_u$  only, but is also consistent with the option that both  $\nu_u$  and  $\nu_\ell$  are shifted by the same average factor as derived for  $L_b$  and  $L_h$  (as van Straaten et al. 2005 reported for SAX J1808.4–3658). This can be seen in Fig. 7b, where  $\nu_u$  and  $\nu_\ell$  of SAX J1808.4–3658 and XTE J1807–294 have been multiplied respectively by 1.454 (the value found by van Straaten et al. 2005) and 1.59 (the weighted average of the  $\nu_b$  and  $\nu_h$  factors; see Table 4). The figure clearly shows that with these shifts the  $\nu_{\ell}$  vs.  $\nu_{u}$  correlation, and for  $\nu_{u} < 600$  Hz also the  $\nu_{b}$  and  $\nu_{h}$  vs.  $\nu_{u}$ correlations, match those in the other sources.

Following van Straaten et al. (2005) and previous works, to prevent crowding of the figures, the  $L_{LF}$  components, with frequencies usually between  $\nu_b$  and  $\nu_h$ , are not displayed in Fig. 7 but their frequencies are plotted vs.  $\nu_h$  separately in Fig. 8. The  $\nu_{LF}$  values we find in XTE J1807–294 are high, above 10 Hz, like in SAX J1808.4–3658 (van Straaten et al. 2005) and in 4U 1820–30 (Altamirano et al. 2005), but are somewhat below the power law extrapolated from the low luminosity bursters.

#### 4. Discussion

We found simultaneous twin kHz QPOs in the power spectra of XTE J1807–294. This is the second accreting millisecond pulsar to show twin kHz QPOs. As the spin period of the neutron star can be inferred precisely and with high confidence from the pulse frequency this provides excellent conditions for testing theoretical models of kHz QPOs (see Section 1; van der Klis 2004 for an overview). In SAX J1808.4–3658 the twin kHz QPO centroids were ~195 Hz apart, consistent with half the inferred spin frequency ( $\nu_{spin} = 401$  Hz) and not with  $\nu_{spin}$  as the original beat-frequency models had predicted (see Section 1). In XTE J1807–294, we find instead that the twin kHz QPO separation is near once the inferred spin frequency.  $\Delta\nu$  is larger than  $\nu_{spin}$  by 2.3 $\sigma$ . This has previously been seen only in 4U 1636–53 (Jonker et al. 2002) and may be difficult to accommodate in beat-frequency (Lamb & Miller 2001) or

relativistic resonance (Kluźniak et al. 2004) models.

In subsequent observations of different sources, a picture is gradually being built up of the relations between the burst oscillation frequency  $\nu_{burst}$ , the pulse frequency  $\nu_{pulse}$ , the kHz QPO separation frequency  $\Delta\nu$ , and the relation of these observed frequencies to the neutron-star spin frequency  $\nu_{spin}$ . We currently have two cases where  $\nu_{burst} \approx \nu_{pulse}$  (and none where these frequencies differ), three examples of  $\Delta\nu \approx \nu_{burst}$  and six examples of  $\Delta\nu \approx \nu_{burst}/2$  (see Table 6). However, so far the only direct information about the relation between  $\nu_{pulse}$  and  $\Delta\nu$  was the one case (SAX J1808.4–3658) where  $\Delta\nu \approx \nu_{pulse}/2$ . The case of XTE J1807–294 constitutes the first example of  $\Delta\nu \approx \nu_{pulse}$ . All these findings are consistent with the simple picture that (i) the pulse frequency is always the spin frequency, (ii) the burst oscillations occur always at the spin frequency, and (iii) for  $\nu_{spin} < 400$  Hz ('slow rotators'),  $\Delta\nu \approx \nu_{spin}$  while for  $\nu_{spin} > 400$  Hz ('fast rotators'),  $\Delta\nu \approx \nu_{spin}/2$ . The strict dichotomy expressed in conclusion (iii) may be due to small sample size; some overlap between the slow and fast rotator groups might well be found in further observations. The model of Lamb & Miller (2003) predicts that kHz QPOs separated by once and half  $\nu_{spin}$  can occur simultaneously, but this has not yet been observed.

In SAX J1808.4–3658, where twin kHz QPOs were detected only once, several commensurabilities between the centroid frequencies of the kHz QPOs and the spin frequency of the form  $\nu_{j,0} = |m\nu_{k,0} - n\nu_{spin}|$  (where  $\nu_{i,0}$  indicates the centroid frequency of component  $L_i$ , j and k designate u and  $\ell$  or vice versa and m and n are integers) were consistent with the data, with in particular  $\nu_{u,0} = |3\nu_{\ell,0} - 2\nu_{spin}|$  a remarkably good match. We searched for this in XTE J1807-294, but with seven detections of kHz QPOs moving over a 200 Hz range in frequency, no commensurabilities remained consistent with the data as the QPOs moved. The data are also not consistent with a constant ratio between kHz QPO centroid frequencies (Table 2). This suggests that, because in SAX J1808.4–3658 only a single twin kHz QPO pair was detected, it was possible for both the commensurability noted by Wijnands et al. (2003) and the 7:4 ratio proposed by Kluźniak et al. (2004) to arise by chance.

The correlations between the frequencies of the several power spectral components detected in LMXBs (cf. Section 1) are a relatively new tool to study these systems, and we are still in the process of figuring out their significance and even their phenomenology. The value that we find for the shift in these correlations ( $\sim$ 1.59) is similar to, but significantly different from, both the value of van Straaten et al. (2005) for SAX J1808.4–3658 ( $\sim$ 1.45) and the small-integer ratio 3/2=1.5 (a value that could suggest a relation with relativistic resonance models; Abramowicz et al. 2003). Yet, the description of the shifts proposed by van Straaten et al. (2005) as the most parsimonious one based on the SAX J1808.4–3658 data (all  $\nu_u$  and  $\nu_\ell$  values are too low by the same factor close to 1.5) provides a remarkable

match to the data also for XTE J1807-294 (Fig. 7b). In SAX J1808.4–3658 only a single  $\nu_{\ell}$  value was available on which to base the conclusion that  $\nu_{\ell}$  was shifted by the same factor as  $\nu_u$ . In XTE J1807-294, blindly applying the same 1.59 shift (derived from the  $\nu_b$  and  $\nu_h$  vs.  $\nu_u$  correlations) to the seven well-distributed  $\nu_{\ell}$  and  $\nu_u$  values, produces a very good match to the atoll-source  $\nu_{\ell}$  vs.  $\nu_u$  relation.

Altamirano et al. (2005) recently reported a similar shift in the frequency correlations of the atoll source 4U 1820-30, but by a factor of  $\sim 1.17$ . This suggests that the mechanism responsible for the shifts may also be present in non-pulsing sources and that the shift factor in  $\nu_u$  may be sometimes far from 1.5. Nevertheless, the small sample size of the 'shifted' sources makes it too early for final conclusions. Descriptions involving different shift factors for different components, and involving shifts of other components than the kHz QPOs are still possible and, indeed, formally required by our fit results (see Table 4). A clear complication is the nature of the shifted correlation diagram (Fig. 7b) at  $\nu_u > 600$  Hz. There, the band-limited noise component labeled  $L_b$  in XTE J1807–294 follows the  $L_{b2}$  track of the atoll sources, and the  $L_h$  track lies above that for the atoll sources or SAX J1808.4–3658. Power law fits to the  $\nu_i$  vs.  $\nu_u$  relations of XTE J1807–294 and the atoll sources (Table 5), show that the slope of the  $\nu_b$  vs.  $\nu_u$  relation in XTE J1807–294 is much less steep than in the other atoll sources, and actually consistent with that of the  $\nu_{b2}$  points (see Fig. 9), and that the  $\nu_h$  points define a steeper relation in XTE J1807–294 than in the other sources. The overall impression created by all of this in Fig. 7b is that of a bifurcation in both the  $\nu_b$  and the  $\nu_h$  vs.  $\nu_u$  relations when  $\nu_u$  exceeds 600 Hz. Perhaps such a bifurcation could be related to the increasing separation between general-relativistic azimuthal and radial epicyclic frequencies when approaching the compact object (e.g., Abramowicz et al. 2003), or to the onset of some form of rotational splitting (cf. Titarchuk & Muslimov 1997), but at this stage this must remain conjectural.

Further analysis of other AMPs and atoll sources is needed to gain a better insight into the frequency correlation shifts. Only a few useful power spectra were obtained up to now for XTE J1751–305, XTE J0929–314 and XTE J1814–338 and no twin kHz QPOs were seen in them. The recent second outburst of XTE J1751–305 (Grebenev et al. 2005; Swank et al. 2005) or forthcoming outbursts of other new or known AMPs can help to give us a more complete view of this shift phenomenon. In any case, our results for XTE J1807–294 when combined with those for SAX J1808.4–3658, strongly support a spin-related mechanism for kHz QPO production and strongly suggest a spin-independent cause of the shift in the frequency correlations. The former is due to the first detection of twin kHz QPOs separated by the spin frequency in a confirmed slow rotator, and the latter to the fact that similar shifts are observed in the frequency correlations of at least two AMPs with very different spin frequencies.

**Acknowledgments:** We thank the referee for valuable comments. ML likes to thank M. Falanga for providing an early copy of his manuscript, and M. Klein-Wolt, T. Maccarone, S.Migliari and R.Wijnands for instructive discussions.

Table 1: Observations used for the timing analysis.

Table 1: Observations used for the timing analysis.							
Set	ObsID	Start date	Det. $a$	PDS $^{b}$	Count rate $(s^{-1})^c$	Bkg. $(s^{-1})^{d}$	
					Total – Per PCU	Total – Per PCU	
A	80145-01-02-00	2003Mar05	3-4	126	266 - 70	102 - 27	
	80145-01-04-03	2003Mar16					
	80145-01-02-03 80145-01-02-02	2003Mar06 2003Mar06					
В	80145-01-02-01	2003Mar06	3-5	99	308 - 78	108 - 27	
	80145-01-03-03	2003Mar $07$					
$\mathbf{C}$	80145-01-01-03 80145-01-01-04	2003Mar01 2003Mar01	4-5	104	391 - 91	115 - 27	
C	80145-01-01-00	2003Mar02	40	104	001 01	110 21	
D	80145-01-01-01	$2003 {\rm Feb28}$	5-5	67	399 - 80	135 - 27	
D	80145-01-03-02	2003Mar $07$	9-9	07	399 – 80	150 - 21	
$\mathbf{E}$	80145-01-02-06	$2003 \mathrm{Mar} 11$	2-4	124	215-74	84-29	
	70134-09-02-00	2003Feb $27$					
F	70134-09-02-01 80145-01-02-04	2003Feb27 2003Mar10	2-5	169	267 - 84	89 - 28	
G	80145-01-03-01	2003Mar12	3-4	87	238 - 70	92-27	
G			0-4	01	200 10	94 41	
Н	80145-01-03-00	2003Mar09	2-4	154	261 - 77	92-27	
	80145-01-02-05	2003Mar13					

<sup>&</sup>lt;sup>a</sup>Minimum and maximum number of active detectors during the observations.

 $<sup>^</sup>b\mathrm{Total}$  number of averaged power density spectra (PDS), each one made from a data segment of 128 seconds.

 $<sup>^</sup>c$ Time averaged count rate not corrected for the background.

 $<sup>^</sup>d\mathrm{Time}$  averaged background count rate estimated with the standard model for bright sources, version 2.1e, provided by the PCA team at GSFC.

Table 2: Twin kHz QPO centroid frequencies with their difference and ratio.

Set	$\nu_{u,0}$ (Hz)	$\nu_{\ell,0} \; (\mathrm{Hz})$	$\Delta \nu^{a} ({\rm Hz})$	$ u_{u,0}/\nu_{\ell,0} $
В	$352.8 \pm 3.5$	$127.1 \pm 28.0$	$225.7 \pm 28.3$	$2.8 \pm 0.6$
$\mathbf{C}$	$374.0 \pm 1.9$	$184.0 \pm 10.5$	$190.0 \pm 10.7$	$2.03 \pm 0.12$
D	$393.4 \pm 3.1$	$195.0 \pm 14.3$	$198.4 \pm 14.6$	$2.02 \pm 0.15$
$\mathbf{E}$	$449.6 \pm 7.1$	$216.5 \pm 23.9$	$233.1 \pm 25.0$	$2.1 \pm 0.2$
F	$466.2 \pm 3.0$	$246.3 \pm 19.0$	$220.0 \pm 19.2$	$1.89 \pm 0.15$
G	$490.6 \pm 4.6$	$253.9 \pm 22.83$	$236.7 \pm 23.3$	$1.93 \pm 0.17$
Н	$563.6 \pm 4.6$	$359.9 \pm 15.8$	$203.7 \pm 16.5$	$1.57 \pm 0.07$

 $<sup>^</sup>a
u_{u,0}$ - $u_{\ell,0}$ 

Table 3: Multilorentzian fits to the power spectra.

	Parameter	$L_b$	$L_{LF}$	$L_h$	$L_\ell$	$L_u$	$\chi^2$ d.o.f.
A	$ \begin{array}{c} \nu_{max}(Hz) \\ Q \\ rms(\%) \end{array} $	5.3±0.6 0 (fixed) 14.56±0.8	$15.6\pm0.6$ $1.4\pm0.3$ $11.6\pm1.2$	$26.8 \pm 0.5 \\ 8^{+15}_{-3} \\ 5.4 \pm 1.0$	$106\pm30$ $0.4\pm0.3$ $15\pm2$	$337\pm10$ $2.8\pm0.6$ $16.7\pm1.5$	180 148
В	$ \begin{array}{c} \nu_{max}(Hz) \\ Q \\ rms(\%) \end{array} $	$5.3\pm0.7$ $0.26\pm0.08$ $11.8\pm0.9$	$14.45 \pm 0.17  9^{+11}_{-3}  4.9 \pm 1.0$	$24.7 \pm 1.6 \\ 0.73 \pm 0.18 \\ 15.9 \pm 1.5$	$163\pm23$ $0.6\pm0.3$ $16\pm2$	$354\pm4$ $5.5\pm1.0$ $15.8\pm1.2$	169 165
C a	$ \begin{array}{c} \nu_{max}(Hz) \\ Q \\ rms(\%) \end{array} $	$6.7\pm0.8$ 0 (fixed) $12.8\pm0.9$	$17.4\pm0.4$ $2.0\pm0.5$ $9.0\pm1.3$	$40\pm 3$ $0.5\pm 0.2$ $16.2\pm 1.9$	$191\pm9$ $1.7\pm0.6$ $12.0\pm1.4$	$375\pm 2$ $6.3\pm 0.5$ $17.3\pm 0.5$	192 143
D	$ \begin{array}{c} \nu_{max}(Hz) \\ Q \\ rms(\%) \end{array} $	$5.7\pm0.7$ $0.45\pm0.16$ $8.8\pm1.4$	$20.2\pm0.4$ $3.6\pm1.2$ $7.8\pm1.2$	44±12 0 (fixed) 20.3±0.9	$202\pm11 \\ 2.0^{+1.2}_{-0.7} \\ 12.1\pm1.9$	$395\pm 3$ $5.1\pm 0.6$ $18.9\pm 0.8$	129 121
E	$ \begin{array}{c} \nu_{max}(Hz) \\ Q \\ rms(\%) \end{array} $	$7.5\pm1.4$ $0.2 \text{ (fixed) }^{b}$ $14.2\pm1.7$	$26.1\pm1.6$ $1.0\pm0.5$ $15\pm3$	- - -	$238\pm25$ $1.2^{+1.2}_{-0.6}$ $17\pm3$	$449\pm9$ $7.9^{+4.4}_{-1.5}$ $15.2\pm1.8$	132 111
F	$ \begin{array}{c} \nu_{max}(Hz) \\ Q \\ rms(\%) \end{array} $	9.4±1.4 0 (fixed) 13.6±1.5	$27.6\pm0.5$ $3.2\pm1.0$ $8.6\pm1.2$	69±23 0 (fixed) 20.3±1.1	$259\pm16$ $1.7\pm0.7$ $13\pm2$	$465\pm 2$ $6.7\pm 0.6$ $18.7\pm 0.7$	202 175
G	$ \begin{array}{c} \nu_{max}(Hz) \\ Q \\ rms(\%) \end{array} $	$7.8\pm1.1$ $0.36\pm0.11$ $14.2\pm1.2$	$32.1\pm1.5$ $1.0\pm0.2$ $16.9\pm1.4$	- - -	$273\pm19$ $1.3\pm0.6$ $20\pm2$	$492\pm 5$ $8\pm 2$ $17.3\pm 1.6$	155 168
Н	$ \begin{array}{c} \nu_{max}(Hz) \\ Q \\ rms(\%) \end{array} $	$10.2\pm0.8$ $0.22\pm0.06$ $16.0\pm0.6$	$40.3\pm1.1$ $1.7\pm0.3$ $13.7\pm1.1$	$129\pm19 \\ 1.2^{+1.4}_{-0.7} \\ 12^{+4}_{-3}$	$370\pm18$ $2.0\pm0.8$ $17\pm3$	$565\pm 5$ $6.6\pm 1.4$ $17.1\pm 1.4$	151 142

 $<sup>^</sup>a\mathrm{An}$  extra component could be added to the fit at  ${\sim}0.1$  Hz, without significant change in the other Lorentzians.

 $<sup>^</sup>b\mathbf{Q}$  fixed to 0.2 for the stability of the fit.

 $<sup>^</sup>c$  This component was  $2.2\sigma$  single trial but when added to the fit function it gave a  $2.9\sigma$  improvement of the chi squared (according to the F-test for additional terms), without significantly changing the rest of the components.

Table 4: Shifts in the frequency-frequency relations in XTE J1807–294.

Component	$\chi^2/d.o.f.$	$\nu_i$ factor	$\nu_u$ factor
$L_{LF}^{a}$	22 / 17	$0.303 \pm 0.031$	$1.725 \pm 0.109$
$L_b$	68 / 22	$0.335 \pm 0.030$	$1.462 \pm 0.048^{b}$
$L_h$	44 / 20	$0.249 \pm 0.017$	$1.715 \pm 0.048^{b}$
$L_{\ell}{}^{c}$	185 / 21	$0.895 \pm 0.083$	$1.082 \pm 0.069$

<sup>&</sup>lt;sup>a</sup>This shift was done using the  $L_{LF1}$  of the low luminosity bursters as a reference (see text and Figure 8)

 $<sup>^</sup>b\mathrm{The}$  weighted average of these two values is 1.59 ±0.03.

 $<sup>^</sup>c A$  double shift in this relation ( $\nu_u$  and  $\nu_\ell$  equally shifted) gave a factor 1.31±0.26, with a  $\chi^2/d.o.f.$  of 185 / 21.

Table 5: Power law fits to the frequency-frequency relations.

$\nu_i = N \times \nu_u{}^\alpha$	α	$\chi^2/d.o.f.$	$\nu_i = N \times \nu_u{}^\alpha$	α	$\chi^2/d.o.f.$
XTE J1807-29	94		Atoll sources		
$ u_b$	$1.29 \pm 0.23$	4 / 6	$ u_b$	$3.072 \pm 0.093$	15 / 14
$ u_{LF}$	$2.169 \pm 0.070$	14 / 6	$ u_{b2}^{a}$	$1.53 \pm 0.39$	9 / 11
$ u_h$	$3.34 \pm 0.33$	9 / 4	$ u_h$	$2.530 \pm 0.074$	29 / 14
$ u_{\ell}$	$1.64 \pm 0.14$	4 / 6	$ u_{\ell}$	$1.402 \pm 0.026$	181 / 14

<sup>&</sup>lt;sup>a</sup>Five  $\nu_{b2}$  values measured by van Straaten et al. (2002, 2003) coincide with the  $L_b$  track at  $\nu_u > 600$  Hz; these were not included in the measurement of the slope of  $\nu_{b2}$  vs.  $\nu_u$ .

Table 6: Approximate relations between the kHz QPO separation  $\Delta\nu$ ,  $\nu_{burst}$  and  $\nu_{pulse}$  in the sources where at least two of these frequencies have been measured. See Table 2.5 in van der Klis 2004 for a more extensive version and complete references.

Source	$\nu_{burst}$ (Hz)	$\nu_{pulse} \; (\mathrm{Hz})$	$\Delta \nu / \nu_{burst}$	$\Delta \nu / \nu_{pulse}$	References	
XTE J1807–294	_	191	_	~1	This paper.	
4U 1915–05	272		$\sim 1$		Galloway et al. (2001)	
XTE J1814–338	314	314			Strohmayer et al. (2003)	
4U 1702–43	330		$\sim 1$		Markwardt et al. (1999)	
4U 1728-34	363		$\sim 1$		Méndez et al. (1999)	
Fast rotators						
SAX J1808.3–3658	401	401	$\sim 1/2$	$\sim 1/2$	Wijnands et al. (2003)	
KS 1731–260	524		$\sim 1/2$		Wijnands & van der Klis (1997)	
Aql X-1	549		$\sim 1/2$		van der Klis $(2000)^a$	
4U 1636–53	582		$\sim 1/2$		Wijnands et al. (1997)	
SAX J1750.8–2900	601		$\sim 1/2$		Kaaret et al. $(2002)^a$	
4U 1608–52	619		$\sim 1/2$		Méndez et al. (1998a,b)	

 $<sup>^</sup>a\mathrm{Marginal}$  detection upper kHz QPO.

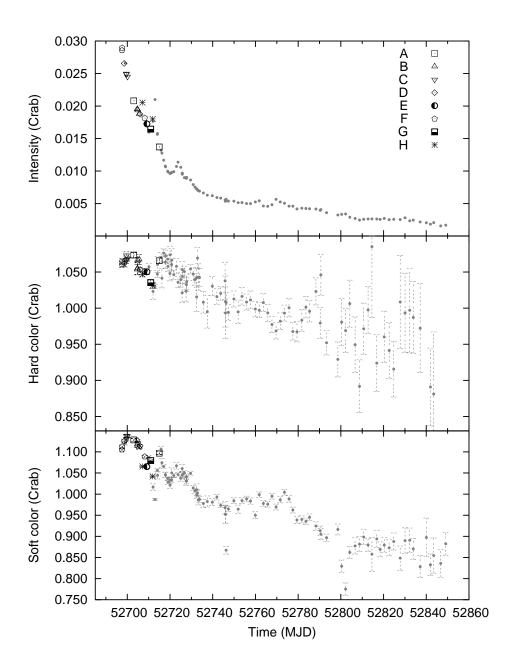


Fig. 1.— Intensity, hard color and soft color (defined in text) versus time for all the observations. Symbols identify the observations used for the timing analysis as indicated. The peak count rate ( $\sim 58$  mCrab) occurred near February  $21^{st}$  (MJD 52691). No strong timing features were detected after March  $23^{th}$  (MJD 52721) because the count rate was too low.

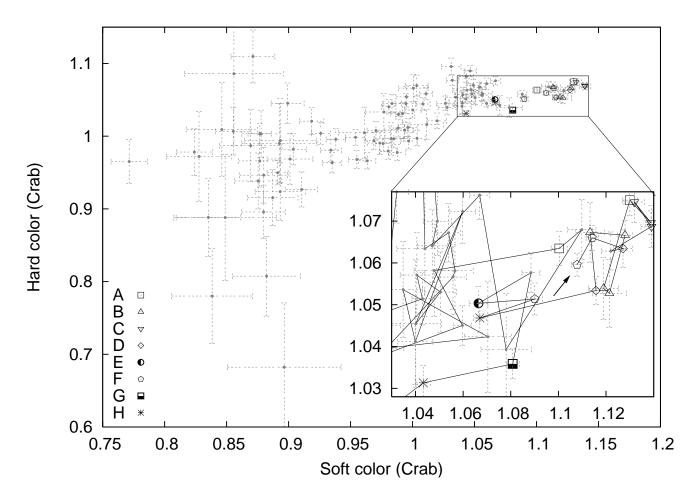


Fig. 2.— Color-color diagram with a zoom into the area used for timing. Symbols identify the observations used for the timing analysis as indicated. The arrow points at the first observation and the solid line indicates the path followed in time.

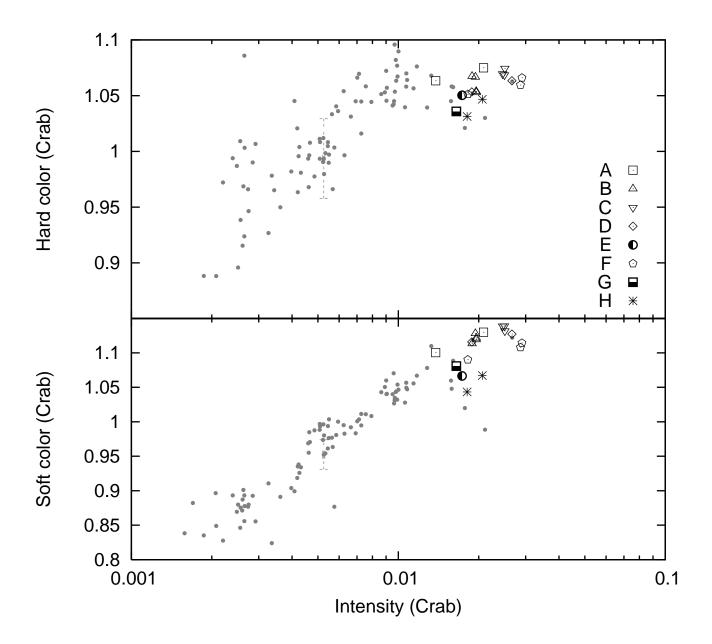


Fig. 3.— Color intensity diagrams. Symbols identify the observations used for the timing analysis as indicated. Typical error bars are shown.

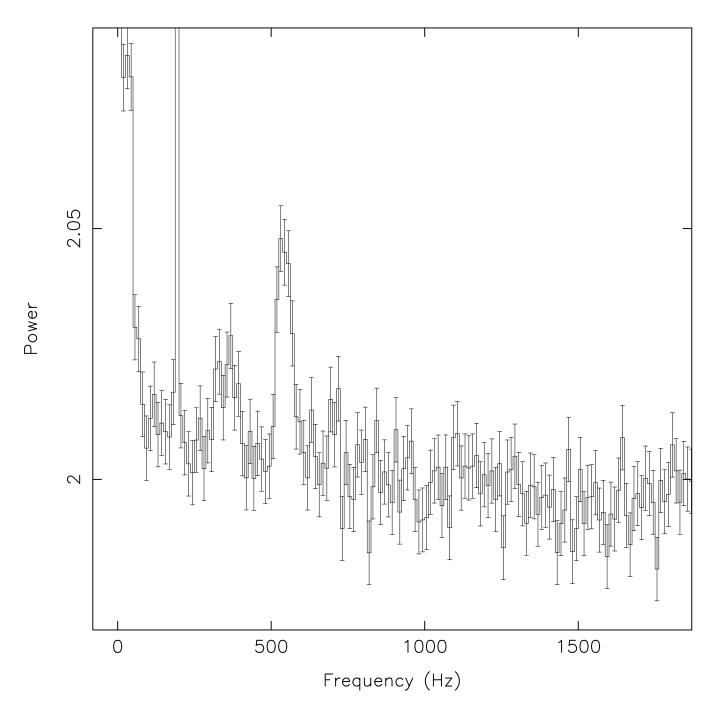


Fig. 4.— Twin kHz QPOs in the power specrum of obs. 80145-01-03-00 (in dataset H). Note the pulsar spike just below  $200~\mathrm{Hz}$ .

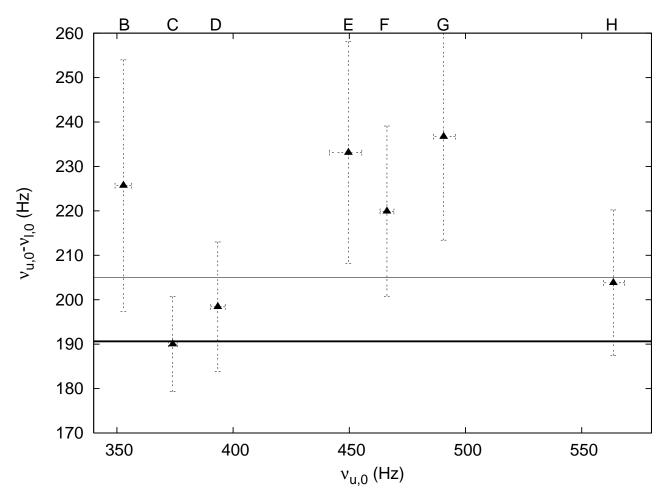


Fig. 5.— kHz QPO frequency separation  $\Delta\nu$  plotted vs.upper kHz QPO centroid frequency  $\nu_{u,0}$ . The thick line indicates the pulse frequency, the thin line the average separation and the letters above the frame the datasets used.

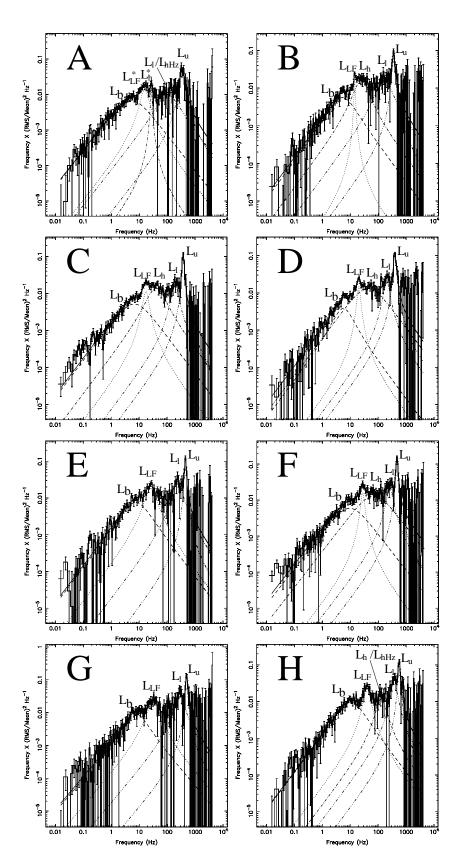


Fig. 6.— Power spectra in power×frequency vs. frequency representation together with the respective fit functions and their Lorentzian components. The pulsar spike was removed before rebinning in frequency.

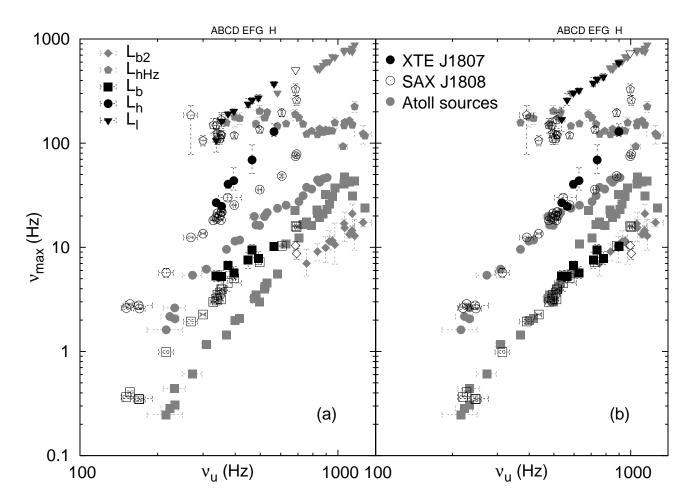


Fig. 7.— Characteristic frequencies of the power spectral components (except  $\nu_{LF}$ , which is analyzed separately) plotted versus the characteristic frequency of the upper kHz QPO. The black symbols correspond to XTE J1807–294, the open ones to SAX J1808.4–3658 and the grey ones to the atoll sources . Symbols identify the different components as indicated, and the letters above the frame the approximate location of XTE J1807–294 data. The observed frequencies are plotted in (a) while in (b) the XTE J1807–294 points were shifted by a factor 1.59 and the SAX J1808.4–3658 points by a factor 1.454 in both  $\nu_u$  and  $\nu_\ell$ . Note the apparent bifurcations in the  $L_b$  and  $L_h$  correlations in (b) for  $\nu_u > 600$  Hz.

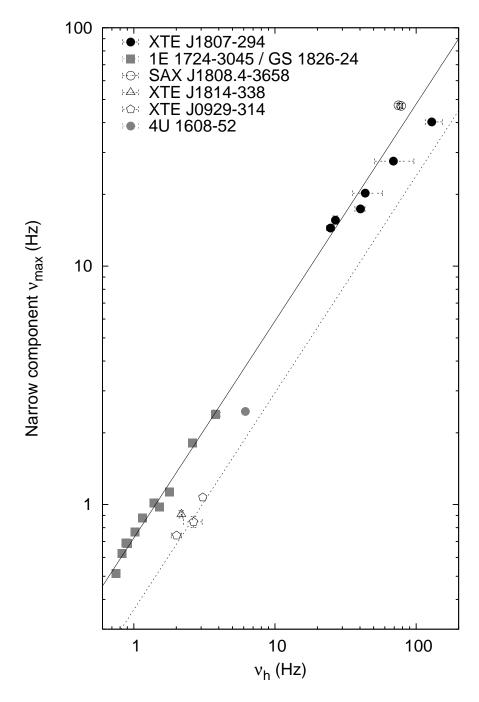


Fig. 8.— Frequencies of  $L_{LF}$  versus the frequencies of  $L_h$ , for the sources indicated in the plot. The solid line shows the power law fit to the low luminosity bursters 1E 1724–3045 and GS 1826–24. The dotted line represents a power law with the same index and a normalization factor half of that of the solid line.

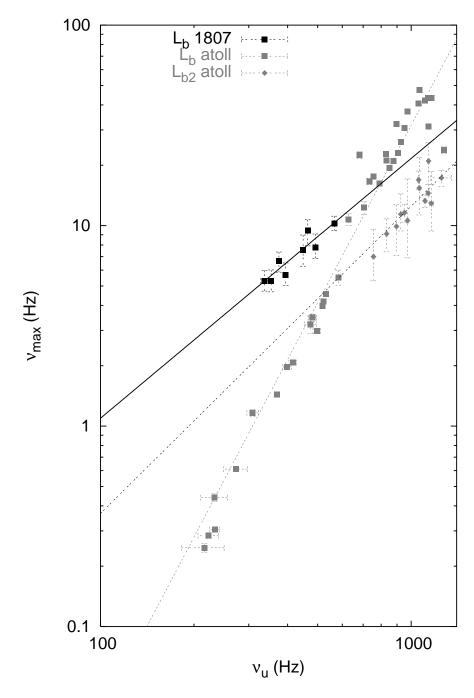


Fig. 9.— Characteristic frequencies of  $L_b$  and  $L_{b2}$  for the atoll sources 4U 0614+09, 4U 1608-52, 4U 1728-34 and Aql X-1 and for XTE J1807-294, plotted versus  $\nu_u$ . The fits to the relations are shown as a solid black line (XTE J1807-294), a dashed black line ( $\nu_{b2}$  of the atoll sources) and a dashed grey line ( $\nu_b$  of the atoll sources). Five points with doubtful identification were excluded (see Table 5).

#### REFERENCES

Abramowicz M.A., Karas V., Kluzniak W., Lee W.H., Rebusco P., 2003, PASJ, 55, 467

Altamirano D., van der Klis M., Mendez M., et al., 2005, ApJ, submitted

Belloni T., Psaltis D., van der Klis M., 2002, ApJ, 572, 392

Campana S., Ferrari N., Stella L., Israel G.L., 2005, astro-ph/0503529

Chakrabarty D., Morgan E.H., Muno M.P., et al., 2003, Nature, 424, 42

Falanga M., Bonnet-Bidaud J.M., Poutanen J., et al., 2005, astro-ph/0503292

Galloway D.K., Chakrabarty D., Muno M.P., Savov P., 2001, ApJ, 549, L85

Galloway D.K., Markwardt C.B., Morgan E.H., Chakrabarty D., Strohmayer T.E., 2005, astro-ph/0501064

Gilfanov M., Revnivtsev M., Sunyaev R., Churazov E., 1998, A&A, 338, L83

Grebenev S.A., Molkov S.V., Sunyaev R.A., Mar. 2005, The Astronomer's Telegram, 446, 1

Hasinger G., van der Klis M., 1989, A&A, 225, 79

Jonker P.G., Méndez M., van der Klis M., 2002, MNRAS, 336, L1

Kaaret P., Zand J.J.M.i., Heise J., Tomsick J.A., 2002, ApJ, 575, 1018

Klein-Wolt M., 2004, Thesis, Universiteit van Amsterdam

Kluźniak W., Abramowicz M.A., Kato S., Lee W.H., Stergioulas N., 2004, ApJ, 603, L89

Kuulkers E., van der Klis M., Oosterbroek T., et al., 1994, A&A, 289, 795

Lamb F.K., Miller M.C., 2001, ApJ, 554, 1210

Lamb F.K., Miller M.C., 2003, astro-ph/0308179

Lee W.H., Abramowicz M.A., Kluźniak W., 2004, ApJ, 603, L93

Markwardt C.B., 2004, In: AIP Conf. Proc. 714: X-ray Timing 2003: Rossi and Beyond, 217–223

Markwardt C.B., Swank J.H., 2003, IAU Circ., 8144, 1

Markwardt C.B., Strohmayer T.E., Swank J.H., 1999, ApJ, 512, L125

Markwardt C.B., Swank J.H., Strohmayer T.E., Zand J.J.M.i., Marshall F.E., 2002, ApJ, 575, L21

Markwardt C.B., Juda M., Swank J.H., Mar. 2003a, IAU Circ., 8095, 2

Markwardt C.B., Smith E., Swank J.H., 2003b, IAU Circ., 8080, 2

Méndez M., van der Klis M., Ford E.C., Wijnands R., van Paradijs J., 1999, ApJ, 511, L49

Méndez M., van der Klis M., van Paradijs J., et al., 1998a, ApJ, 494, L65+

Méndez M., van der Klis M., Wijnands R., et al., 1998b, ApJ, 505, L23+

Miller M.C., Lamb F.K., Psaltis D., 1998, ApJ, 508, 791

Press W.H., Teukolsky S.A., Vetterling W.T., Flannery B.P., 1992, Numerical recipes in FORTRAN. The art of scientific computing, Cambridge: University Press, —c1992, 2nd ed.

Psaltis D., Belloni T., van der Klis M., 1999, ApJ, 520, 262

Remillard R.A., 2002, IAU Circ., 7888, 2

Stella L., Vietri M., 1998, ApJ, 492, L59+

Strohmayer T.E., Zhang W., Swank J.H., et al., 1996, ApJ, 469, L9+

Strohmayer T.E., Markwardt C.B., Swank J.H., in't Zand J., 2003, ApJ, 596, L67

Swank J.H., Markwardt C.B., Smith E.A., Mar. 2005, The Astronomer's Telegram, 449, 1

Titarchuk L., Muslimov A., 1997, A&A, 323, L5

van der Klis M., 1995, Proceedings of the NATO Advanced Study Institute on the Lives of the Neutron Stars, held in Kemer, Turkey, August 19-September 12, 1993. Editor(s), M. A. Alpar, U. Kiziloglu, J. van Paradijs; Publisher, Kluwer Academic, Dordrecht, The Netherlands, Boston, Massachusetts, 301

van der Klis M., 2000, ARA&A, 38, 717

van der Klis M., 2004, astro-ph/0410551

van Straaten S., van der Klis M., di Salvo T., Belloni T., 2002, ApJ, 568, 912

van Straaten S., van der Klis M., Méndez M., 2003, ApJ, 596, 1155

van Straaten S., van der Klis M., Wijnands R., 2005, ApJ, 619, 455

Vanderspek, R. and Morgan, E. and Crew, G. and Graziani, C. and Suzuki, M., Jun. 2005, The Astronomer's Telegram, 516, 1

Wijnands R., 2005, astro-ph/0501264

Wijnands R., van der Klis M., 1998, Nature, 394, 344

Wijnands R., van der Klis M., 1999, ApJ, 514, 939

Wijnands R., van der Klis M., Homan J., et al., 2003, Nature, 424, 44

Wijnands R.A.D., van der Klis M., 1997, ApJ, 482, L65+

Wijnands R.A.D., van der Klis M., van Paradijs J., et al., 1997, ApJ, 479, L141+

Zhang W., Jahoda K., Swank J.H., Morgan E.H., Giles A.B., 1995, ApJ, 449, 930

This preprint was prepared with the AAS LATEX macros v5.2.